Protein Science (2000), *9*:1374–1381. Cambridge University Press. Printed in the USA.
Copyright © 2000 The Protein Society

The X-ray structure of the NAD-dependent 5,10-methylenetetrahydrofolate dehydrogenase from *Saccharomyces cerevisiae*

ARTHUR F. MONZINGO, ANDREW BREKSA, STEPHEN ERNST, DEAN R. APPLING, AND JON D. ROBERTUS

Department of Chemistry and Biochemistry, University of Texas at Austin, Austin, Texas 78712

(RECEIVED February 8, 2000; FINAL REVISION April 17, 2000; ACCEPTED April 28, 2000)

Abstract

Eucaryotes possess one or more NADP-dependent methylene-THF dehydrogenases as part of multifunctional enzymes. In addition, yeast expresses an unusual monofunctional NAD-dependent enzyme, yMTD. We report X-ray structures for the apoenzyme and its complex with NAD^+ at 2.8 and 3.0 Å resolution, respectively. The protein fold resembles that seen for the human and *Escherichia coli* dehydrogenase/cyclohydrolase bifunctional enzymes. The enzyme has two prominent domains, with the active site cleft between them. yMTD has a noncanonical NAD-binding domain that has two inserted strands compared with the NADP-binding domains of the bifunctional enzymes. This insert precludes yMTD from dimerizing in the same way as the bifunctional enzymes. yMTD functions as a dimer, but the mode of dimerization is novel. It does not appear that the difference in dimerization accounts for the difference in cofactor specificity or for the loss of cyclohydrolase activity. These functional differences are probably accounted for by minor differences within the tertiary structure of the active site of the monomeric protein.

Keywords: NAD dependent; nonstandard NAD domain; novel dimerization; THF dehydrogenase; X-ray structure

Serine, derived from glycolytic intermediates, is the major source of one-carbon units used for biosynthesis in most organisms (Schirch, 1984). The serine 3-carbon is transferred to tetrahydrofolate (THF) to generate 5,10-methylene-THF and glycine. This form of the coenzyme is used directly for thymidylate synthesis or can be reduced to 5-methyl-THF, to be used for methyl group biogenesis. In rapidly growing cells, the synthesis of purines is a critical folate-dependent pathway, requiring 2 mol of 10-formyl-THF per mol of purine ring.

5,10-Methylene-THF is converted to 10-formyl-THF via the sequential action of enzymes 5,10-methylene-THF dehydrogenase (Reaction 1) and 5,10-methenyl-THF cyclohydrolase (Reaction 2):

$$\text{5,10-methylene-THF} + \text{NAD(P)}^+ \Leftrightarrow \text{5,10-methenyl-THF} + \text{NAD(P)H} \quad (1)$$

$$\text{5,10-methenyl-THF} + \text{H}_2\text{O} \Leftrightarrow \text{10-formyl-THF}. \quad (2)$$

Methylene-THF dehydrogenase (EC 1.5.1.5), abbreviated MTD, is typically found as part of a multifunctional protein in eukaryotes. NADP-dependent methylene-THF dehydrogenases in mammals, birds, and yeast are components of a trifunctional enzyme called C_1-THF synthase that also contains methenyl-THF cyclohydrolase and 10-formyl-THF synthetase activities (MacKenzie, 1984). In these eukaryotic enzymes (subunit M_r = 100,000), the dehydrogenase and cyclohydrolase activities are contained in a 30–35 kDa N-terminal domain, and the synthetase activity is located in a 70 kDa C-terminal domain. Certain eukaryotic cells also contain a 34 kDa homodimeric bifunctional NAD-dependent methylene-THF dehydrogenase/methenyl-THF cyclohydrolase (MacKenzie, 1997). These bifunctional enzymes are referred to as MTD/Cs. This enzyme requires both Mg^{2+} and inorganic phosphate (Yang & MacKenzie, 1993) and is restricted to the mitochondria of undifferentiated cells (Mejia & MacKenzie, 1985). In bacteria, monofunctional NAD- and NADP-dependent methylene-THF dehydrogenases, as well as bifunctional NADP-dependent methylene-THF/methenyl-THF cyclohydrolase enzymes are found. All of these prokaryotic enzymes exist as homodimers of subunit M_r = 30–35,000.

In addition to the more common trifunctional enzyme, *S. cerevisiae* also expresses an NAD-dependent 5,10-methylene-THF dehydrogenase activity in the cytoplasm (Barlowe & Appling, 1990), encoded by the *MTD1* gene (West et al., 1993). In contrast to all other eukaryotic methylene-THF dehydrogenases characterized to date, this enzyme appears to be monofunctional, lacking cyclo-

Reprint requests to: Jon Robertus, Institute of Cellular and Molecular Biology, Department of Chemistry and Biochemistry, University of Texas, Austin, Texas 78712; e-mail: jrobertus@mail.utexas.edu.

hydrolase activity. This dehydrogenase is specific for NAD^+ and is not dependent on Mg^{2+} or phosphate for activity. The enzyme is a homodimer with a subunit molecular mass of 36 kDa (320 amino acids), reminiscent of the dehydrogenase/cyclohydrolase domain of the trifunctional C_1-THF synthase. However, the deduced amino acid sequence shows only slight (18–25%) similarity to other methylene-THF dehydrogenase sequences (Appling & West, 1997).

Here we describe the structure of this monofunctional enzyme from yeast (yMTD) and compare it to the recently reported structures of the dehydrogenase/cyclohydrolase domain from the human C_1-THF synthase, that is, the N-terminal 301 residues, abbreviated hMTD/C (Allaire et al., 1998) and the bifunctional dehydrogenase/cyclohydrolase from *Escherichia coli*, abbreviated eMTD/C (Shen et al., 1999).

Results and discussion

Structure determination

Three-dimensional data for yMTD are summarized in Table 1. The Ramachandran plot has 80% of residues in the most favorable region, 17% in additional allowed space, 2% in generously allowed space, and one residue (Asn184) in the disallowed space. The asparagine residue replaces a glycine usually found in NAD-binding domains and thus may be constrained to an unfavorable conformation.

The refined model of yMTD includes residues 3–319. Residue 1 is a Met, which is probably processed away from the expressed protein. Residues 2 and 320, not visible in the electron density maps, are most likely disordered and have not been built into the model. Residues 3, 318, and 319 have been modeled as alanines because their side chains cannot be seen in the electron density maps. As described in Materials and methods, the electron density corresponding to several stretches of the chain was not interpretable in the initial MAD-phased map. With the exception of the terminal amino acids, these residues (3–6, 230–237, 280–286, and 317–319) have been modeled from later electron density maps but have higher average temperature factors (59.4 $Å^2$ for main-chain atoms) than that for the entire molecule (42.8 $Å^2$). The relatively high thermal motion of the molecule is consistent with the difficulty in measuring high-resolution data, even with a synchrotron source. It is most likely responsible for the high free *R*-values for the model.

A section of the final electron density map is shown in Figure 1.

Table 1. *Crystallographic data*

	Native	Se	NAD
Resolution (Å)	2.8	2.8	2.9
R_{merge} (%)	9.2	4.5	7.7
R_{merge} (last shell) (%)	26.3	36.0	57.8
$\langle I/\sigma_I \rangle$	12.0	23.1	11.3
$\langle I/\sigma_I \rangle$ (last shell)	3.1	2.4	2.1
Completeness (%)	97.8	81.1	81.3
Completeness ($I/\sigma_I > 5$) (%)	61.3	53.2	50.0
Completeness ($I/\sigma_I > 5$) (last shell) (%)	19.6	9.9	8.7
Unique reflections	10,691	17,232	8474
Redundancy	4.8	1.8	3.3
Wavelengths (Å)	1.5418	0.978641	1.5418
		0.97928	
		0.95001	
SOLVE $\langle m \rangle$		0.58	
Phasing FOM		0.754	
Phasing power		1.82	
Number of residues	317		317
Number of atoms	2534		2574
$R_{working}$	0.26		0.25
R_{free}	0.35		0.36
RMSD from ideality			
Bonds	0.005		0.004
Angles	1.217		1.216

Structure of yMTD

yMTD folds into two structural domains separated by a large active site cleft. Figure 2 shows a ribbon drawing of the protein, emphasizing the cleft formed between the smaller N-terminal domain and the larger C-terminal NAD-binding domain. Table 2 lists the secondary structural elements of the protein.

The two major domains of yMTD are secured by the interaction of two long helices A and I. These helices, from opposite ends of the molecule, lie roughly parallel to one another and make numerous interactions.

The body of the N-terminal domain consists roughly of residues 31–124 and contains three α-helices (B, C, and D) and a three-stranded (b, c, and d) mixed β-sheet. Residues 125–147, containing helix E, forms a small module that interacts with the two major domains. The large NAD-binding domain contains a prominent eight-stranded β-sheet composed of strands e–k and strand a from the N-terminus.

Comparison with MTD/Cs

yMTD has an overall folding pattern very similar to the dehydrogenase/cyclohydrolase domain from the human trifunctional enzyme (Allaire et al., 1998) and to the bifunctional enzyme from *E. coli* (Shen et al., 1999). The alignment of amino acid sequences of these enzymes is shown in Figure 3. Figure 4 shows a least-squares superposition of the Cα backbone of yMTD with that of the hMTD/C (Protein Data Bank (PDB) ID 1A4I). The crystal structure of hMTD/C has two molecules in the asymmetric unit, and the comparison in Figure 4 is between yMTD and unit 1 of hMTD/C. The orientation is roughly 90° from that in Figure 2, looking into the NAD-binding site. In this view, corresponding α-carbons from the larger NAD-binding domains were aligned in a least-squares sense. The root-mean-square deviation (RMSD) of 103 common α-carbons in the NAD-binding domains is 1.3 Å. It is clear that most secondary structural elements in the large NAD binding domain, such as the β-sheet of the domain, align closely between the two proteins. The smaller amino terminal domains of the two proteins do not superimpose as perfectly; and in this orientation, the RMSD of the N-terminal domains is 4.8 Å. However, the overall shape of the smaller N-terminal domains is very similar, and they can be independently aligned so that the RMSD of 81 common α-carbons is 1.1 Å.

When the full proteins are aligned based on their NAD-binding domains, it is clear that the amino terminal domain of yMTD has been displaced as a nearly rigid group with respect to that domain in the hMTD/C. This is easy to see in Figure 4 by noting that three

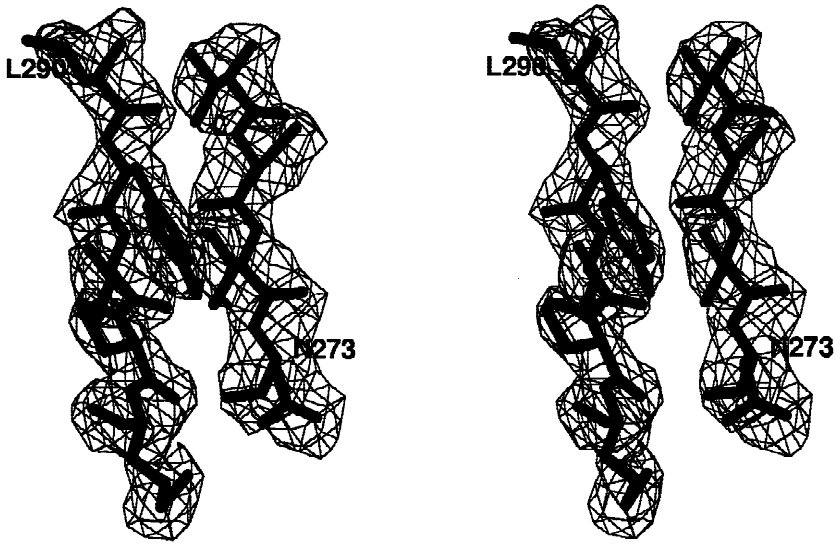

Fig. 1. A $2F_o - F_c$ electron density map for yMTD. Residues 270–273 and 290–294 are superimposed on their electron density. The density baskets enclose values above 1σ.

α-helices in the yMTD N-terminal domain are roughly perpendicular to our view, and their movement to the hMTD/C position can be readily discerned. The exact motion is not easy to describe and is complicated by the fact that the amino acid sequences and loop sizes differ between the proteins. However, a first approximation to the domain motion can be seen by noting that the α-carbons of Met64 in yMTD and Ile63 of the human enzyme nearly superimpose at the base of helix B (see Fig. 4). The top of the helix in hMTD/C is tilted by 11° compared to that in yMTD; a similar tilt is seen for the β-sheet of the N-terminal domain.

The asymmetric unit of hMTD/C is a dimer in which the two molecules differ slightly in structure, and, in particular, in the orientation of the N-terminal domains with respect to the NAD domains (Allaire et al., 1998). When the NAD domain of yMTD is aligned with that of the second molecule of the hMTD/C dimer, the motion of the N-terminal domain is more pronounced than that shown in Figure 4 for molecule 1. In the second case, the tilt angle for the B-helix is about 16°, and there is also a translation of ~3 Å. This difference reinforces the notion (Allaire et al., 1998) that the hinge between the two domains is fairly flexible in this enzyme class and can probably move to accommodate binding of the tetrahydrofolate substrate.

The sequence alignment shown in Figure 3 reveals several prominent insertions and deletions between yMTD and the hMTD/C

Fig. 2. A ribbon drawing of yMTD. The observed binding of NAD^+ is shown in solid black bonds.

Table 2. *Secondary structure for yeast MTD*

α-Helix	Residues	β-Strand	Residues
A1	9–15	a	6–8
A2	17–31	b	37–43
B	47–63	c	67–73
C	76–88	d	94–98
D	104–113	e	179–184
E	125–133	f	203–207
F	149–162	g	212–216
G	189–199	h	227–232
H	236–245	I	247–251
I	296–317	j	270–274
		k	290–292

Fig. 3. Amino acid sequence alignments of MTDs. yMTD is the monofunctional enzyme from yeast, hMTD/C is the dehydrogenase/cyclohydrolase fragment from humans, and eMTD/C is the dehydrogenase/cyclohydrolase enzyme from *E. coli*. Residues invariant in the three proteins are shown as bold type. The sequence numbers are those of yMTD. Insertions and deletions are positioned based on the X-ray models.

proteins. yMTD residues 139–145 represent an insertion; this added loop is labeled with the E141 marker (Fig. 4). Inserted residues 165–173 are around the back of the molecules in Figure 4 and are not clearly visible and therefore not labeled. A 25-residue insertion, residues 211–235, is marked in Figure 4 by K222; this large insertion contains strands g and h in yMTD and plays a key role in determining differences in dimerization between yMTD and the two bifunctional proteins. Finally, the bifunctional molecules have a substantial insertion between yMTD residues 281 and 282. In Figure 4, this large inserted loop is denoted by the *R250* marker attached to the hMTD/C. Arg250 of hMTD/C is marked in Figure 3 in bold italics.

Nucleotide-binding domain

Strands e through k are part of a noncanonical nucleotide-binding domain. This is shown in more detail in Figure 5. Strand e, helix G, and strand f form a standard binding motif for the adenosine moiety. In a canonical nucleotide-binding domain, strand f would be followed by a return α-helix on the far side of the sheet and parallel to G. Instead, the return β strand, g, hydrogen bonds into the sheet in an antiparallel fashion. Strand h finishes the first half of the sheet by forming an antiparallel interaction with g instead of the usual, canonical, parallel interaction with f. Helix H then crosses back to set up the nicotinamide binding motif composed of parallel strands i, j, and k. There are no extended α-helical returns following these strands, but the chain between strands i and j and between j and k contain short irregular helical stretches, suggesting they may have arisen from the more common nucleotide-binding fold.

The bifunctional enzymes for human and *E. coli* also have noncanonical nucleotide-binding domains, but they differ from yMTD in their topology. In both former cases, the β-sheet is truncated to a five-stranded structure. In particular, they lack the analog of yMTD strands g and h; instead, they fold in such a way that the equivalent strand to f connects directly to the cross-over helix, H in Figure 5. The presence of strands g and h marks one of the more profound structural differences between yMTD and the bifunctional enzymes.

Many enzymes with NAD-binding domains exhibit a characteristic signature GXGXXG sequence (Rossmann et al., 1975). How-

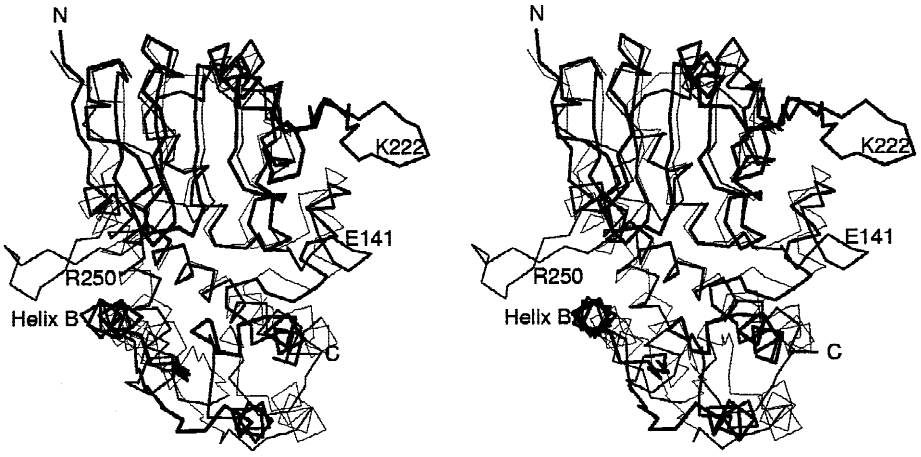

Fig. 4. A least-squares superposition of yMTD and human MTD/C. The Cα traces are shown, with the yeast enzyme in the thicker bonds and the hMTD/C in thin bonds. The NAD binding domains have been aligned in a least-squares sense. Protein 1 of the hMTD/C dimer is shown, although residues 241–250, not visible in unit 1, are those from unit 2.

ever, it is increasingly common to see NAD binding domains that lack this sequence, such as the seven residue GXXGXXG motif seen in malate dehydrogenase (Birktoft et al., 1989). The yMTD NAD-binding domain, like the bifunctional enzymes, does not have the archetypal signature sequence. hMTD/C uses residues 172–178 (GRSKIVG) and yMTD uses the corresponding residues 184–190 (NRSEIVG) to interact with the adenine moiety. Generally, NAD-binding enzymes have an Asp or Glu at the C-terminus of the second β-strand on the nucleotide-binding domain (f) that hydrogen bonds to the 2′ and/or 3′ hydroxyls of the ribose; that role is played by Asp208 in yMTD. The bifunctional enzymes bind NADP and lack this residue. Instead, those enzymes have cationic residues that act as counterions to the 2′ phosphate of the cofactor. Such a role in the human enzyme is played by Lys198 together with Arg173 (Allaire et al., 1998) and by Arg191 in the bacterial bifunctional enzyme (Shen et al., 1999).

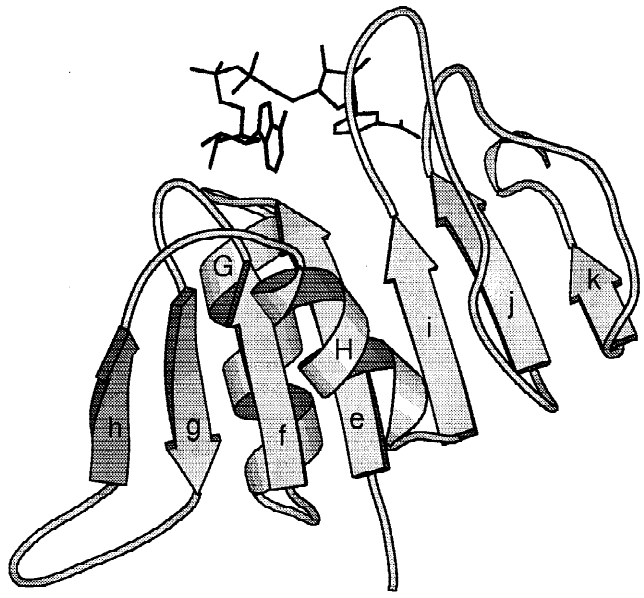

Fig. 5. Details of the yMTD NAD-binding domain. A ribbon drawing of the secondary structural arrangement of the NAD-binding domain is shown, with segments labeled.

Data were collected from a crystal of yMTD soaked with NAD^+. The electron density corresponding to the adenine moiety was clear and well defined, allowing that half of the cosubstrate to be positioned with confidence. Density corresponding to the nicotinamide was weak, suggesting that the group was in motion or otherwise disordered. Given the fixed position of the adenosine moiety in yMTD, the nicotinamide group was positioned in a manner based on that seen in the crystal structure of hMTD/C. This is consistent with what little electron density is observed in the yMTD map. It also makes interaction between the nicotinamide ring and several amino acids conserved between the two proteins including T151 (T148 in human), V189 (V177 in human), and G296 (G276 in human). It is likely that the nicotinamide group would be oriented more definitively in the presence of a methylene tetrahydrofolate substrate, or analog. Unfortunately, we have so far been unable to crystallize such a ternary complex.

yMTD dimerization

Like the bifunctional enzymes, yMTD functions as a homodimer (Barlowe & Appling, 1990). The crystallographic asymmetric unit of the yMTD crystal is a monomer, suggesting that a true molecular twofold axis within the homodimer is aligned with a crystallographic twofold. The crystal contains several classes of twofold operators, but one makes significantly greater contacts between molecules than the others and is assumed to represent the molecular twofold. This aggregation differs from that seen for the human and bacterial enzymes. Those enzymes dimerize in such a way that the exposed edge (strand f) of the NADP-binding β-sheets align in an antiparallel fashion. This forms a continuous sheet between the two molecules of the dimer. Such an alignment is unlikely for yMTD because the extra strands, g and h, of the NAD binding domain protrude from the body of the molecule and would allow only a weak interaction. (None of the crystallographic twofolds in the yMTD cell produce packing similar to the human or bacterial

dimers.) Calculations using the program GRASP (Nicholls et al., 1991) reveal that 1,066 Å^2 of solvent-accessible surface per monomer is buried upon dimerization. The suspected mode of dimerization of yMTD and a comparison with the dimerization of hMTD/C is shown in Figure 6.

It is tempting to ask if the difference in dimerization of the monofunctional yMTD and the bifunctional enzymes might be related to the loss of cyclohydrolase activity. As will be described below, we consider this to be unlikely. It is, however, unclear why the two classes of enzymes function as dimers and why the modes of dimerization differ. At this time, none of the MTD enzymes has been seen with a folate substrate bound, although a hypothetical model of such an interaction has been proposed (Shen et al., 1999). It may be that future work will reveal a role for the dimer in substrate recognition.

Cyclohydrolase activity

A principal difference between yMTD and the bifunctional enzymes is the lack of cyclohydrolase activity in the former. The cyclohydrolase reaction itself is thermodynamically favorable, and is kinetically very facile; the buffer-catalyzed rate is generally significant compared to the enzyme-catalyzed reaction (Robinson, 1971). It has been suggested from metabolic and genetic experiments that the NAD-dependent yMTD may function in the oxidative direction, taking the methylene-THF to formyl-THF, while the eucaryotic trifunctional enzymes may function primarily in the reductive direction (West et al., 1996). A recent kinetic analysis of the MTD/C enzymes is consistent with this notion (Pawelek & MacKenzie, 1998). It showed that the cyclohydrolase reaction is rate limiting in the reductive direction, while hydride transfer is rate limiting in the oxidative direction. Because yMTD functions exclusively in the oxidative direction, it could lose the cyclohydrolase reaction because the spontaneous hydrolysis of its 5,10-methenyl-THF product is faster than the rate limiting catalytic step.

A comparison of yMTD and the MTD/C enzymes may shed light on the reactive groups of the cyclohydrolase step. The cyclohydrolase active site is thought to exist on the small N-terminal domain of the bifunctional enzymes (Allaire et al., 1998). Key residues may include Ser49, Tyr52, Lys56, and Gln100; the suspected attacking water molecule in the cyclohydrolase reaction is thought to be hydrogen-bonded to the side chains of Ser49 and Gln100. These residues are replaced by Ala50 and Tyr98 in yMTD, and Lys56 is changed to Thr57. The electron density map shows no water in a comparable site to that seen in the bifunctional enzymes. This is not a proof that the hypothesized cyclohydrolase site is correct, but our observations are consistent with that notion.

Materials and methods

The yeast monofunctional cytoplasmic MTD was purified as previously reported (Appling & West, 1997). The crystallization of the protein has been described previously (Monzingo et al., 1996).

yMTD containing selenomethionine was prepared generally following the method of Hoffman et al. (1994). The plasmid pET-

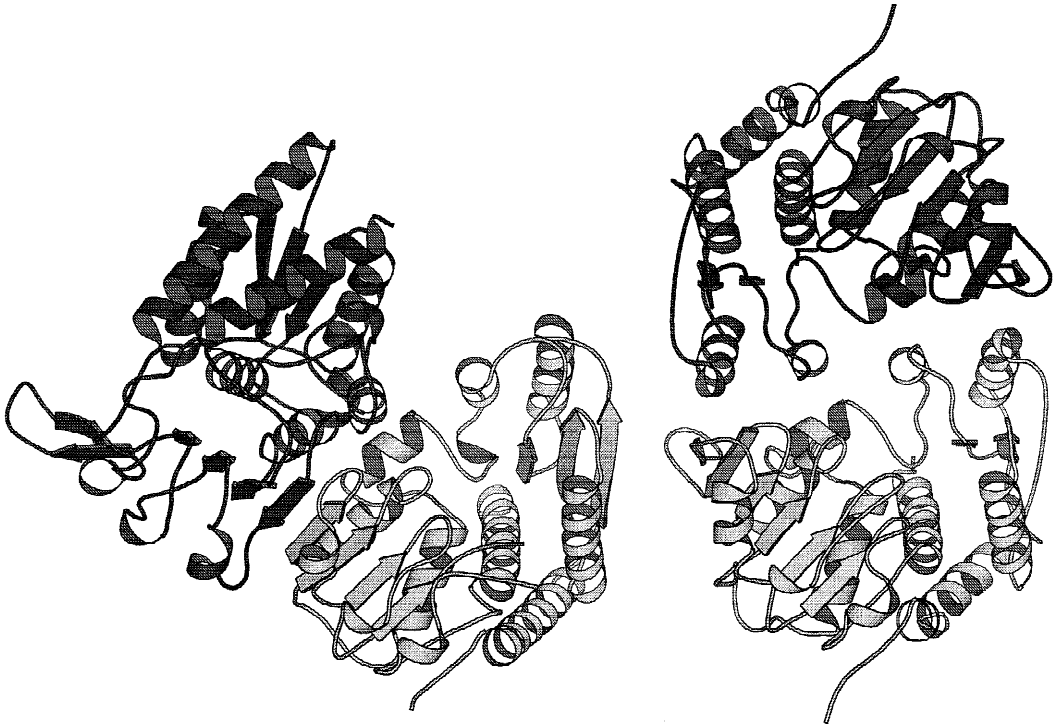

Fig. 6. Dimerization of yMTD and hMTD/C. Ribbon drawings are used to show each dimer. yMTD is on the right side of the picture with one monomer as a light colored ribbon and one as a darker ribbon. The view is down the molecular twofold axis. The hMTD/C dimer is on the left, with the light colored monomer aligned, in a least-squares sense, with the light monomer of yMTD. Note that the hMTD/C dimerization involves the extended β-sheets of the NAD binding domains (lower left).

MTD (Appling & West, 1997), which contains the open reading frame (ORF) of *MTD1* under the control of an inducible promoter and the gene for ampicillin resistance, was transformed into *E. coli* methionine auxotrophic strain B834(DE3) (Novagen Corp., Madison, Wisconsin). Cells were grown in defined medium containing the following components (per liter): 12 g Na_2HPO_4, 6 g KH_2PO_4, 2 g NH_4Cl, 1 g NaCl, 4 g dextrose, 100 mg ampicillin, 1 mg biotin, 1 mg choline chloride, 1 mg folic acid, 1 mg niacinamide, 1 mg D-pantothenate, 1 mg pyridoxal, 0.1 mg riboflavin, 5 mg thiamine, 2 mM $MgSO_4$, 1 μM $FeCl_3$, 0.2 mM $CaCl_3$, 40 mg/L of each amino acid apart from methionine and 40 mg/L L-selenomethionine (Sigma Chemical Co., St. Louis, Missouri). Cells were first inoculated into 2 mL of the medium containing 100% methionine, and this culture was then sequentially diluted (100:1) into cultures containing 50, 80, and 100% selenomethionine. Finally, the last culture was diluted into a 4 mL culture containing 100% selenomethionine, and this culture was used to inoculate a 1.2 L culture. Cells were grown to an optical density of 1.0 at 600 nm and induced with isopropyl-β-D-thiogalactopyranoside (IPTG) to a final concentration of 1 mM. After a 12 h induction, the cells were harvested by centrifugation for 20 min at 7,000 $\times$ *g*. The selenomethionine-substituted yMTD (syMTD) was purified as described for the wild-type (Barlowe & Appling, 1990). Crystals of syMTD were prepared in sitting drops as described for the native (Monzingo et al., 1996).

Prior to data collection, crystals were treated with cryoprotectant, either by transfer to artificial mother liquor (8% PEG 8000, 50 mM Tris-HCl, pH 8.2) containing 35% glycerol for 1–5 s or by transfer to artificial mother liquor containing increasing amounts of glycerol up to 35% in steps of 5% (5 or more minutes per step). Crystals, mounted in a cryoloop (Hampton Research, Laguna Niguel, California), were frozen by dipping in liquid nitrogen and placed in the cold stream on the goniostat.

A Hg derivative crystal was prepared by soaking an syMTD crystal in artificial mother liquor containing 1 mM *p*-chloromercuriphenylsulfonic acid (Sigma Chemical Co.) for 18 h. A Pt derivative crystal was prepared by soaking an syMTD crystal in artificial mother liquor containing 5 mM potassium tetranitritoplatinite (Apache Chemicals, Seward, Illinois) for 12 h. An MTD crystal with bound NAD was prepared by soaking a native crystal in artificial mother liquor containing 5 mM NAD (Sigma Chemical Co.) for 2 weeks.

Native data and data from the NAD derivative were collected at 100 K on a Rigaku Raxis IV with X-rays generated by a Rigaku SU-200 rotating anode generator operated at 50 mV, 100 mA. MAD data of the syMTD native, Hg derivative, and Pt derivative were collected at 100 K on beamline X-12C at the National Synchrontron Light Source, Brookhaven National Laboratory. Data from three different wavelengths were collected on each crystal; the choices of wavelength were optimized by an analysis of the absorption spectrum for each crystal (Ramakrishnan & Biou, 1997). Diffraction images were processed using DENZO, and data were reduced using SCALEPACK (Otwinowski & Minor, 1997).

Six selenium sites were determined from the syMTD native MAD data using SOLVE (Terwilliger & Berendzen, 1999). MAD phasing was done with MLPHARE (CCP4, 1994). Solvent-flattening of the native was done with DM (CCP4, 1994). The solvent-flattened map was skeletonized with MAPMAN (Kleywegt & Jones, 1996). Statistics from DM, as well as the handedness of helices observed in skeletonized maps, were used to correctly assign the hand of the reciprocal lattice and the Se sites and to determine the space group ($P4_12_12$ rather than $P4_32_12$). The backbone of the protein was traced from the solvent-flattened map using the skeleton along with the baton_build feature of O (Jones et al., 1991). Difference Fouriers with the Hg and Pt data revealed two Hg sites and two Pt sites. The Pt sites were near known Se sites. The Se and Hg sites were used to mark the six methionine and two cysteine residues, respectively, in assigning the amino acid sequence to the chain trace.

The initial model, which consisted of 292 residues and did not include residues poorly defined in the electron density map (residues 1–6, 230–237, 273–286, and 317–320), was refined using the slow-cooling protocol of X-PLOR (Brünger, 1992). The refined model had a working *R*-factor of 0.35 and an R_{free} of 0.52 (5–2.9 Å). To facilitate manual rebuilding of the model, a difference map and a $2F_o - F_c$ map, weighted to eliminate bias from the model, were prepared. A difference map of the form $(F_o - F_c)\alpha_{calc}$ was calculated using X-PLOR. To prepare the unbiased $2F_o - F_c$ map, structure factors, and phases based on the model were calculated with X-PLOR then analyzed by LBEST to generate weights based on the free *R*-value (Brünger, 1993; Lunin & Skovoroda, 1995; Urzhumtsev et al., 1996). Fourier maps using amplitudes of the form $|2wF_o - DF_c|$, where *w* and *D* are weights determined by LBEST, and phases calculated from the model were then generated by FFT (CCP4, 1994). Using these maps, the model was rebuilt to better fit the electron density. Model building was done on a Silicon Graphics Indy computer using O. Other computations were done on an Alpha computer (Digital Equipment Company).

After several rounds of rebuilding and refinement, the electron density had improved so that the gaps corresponding to missing residues could be built in the model. At this point, the model consisted of 315 residues ($R_{work} = 0.24$, $R_{free} = 0.36$; 8–3.0 Å). For the final stages of refinement, an anisotropic *B*-factor correction was made to the observed native modulus structure factors, and a bulk solvent correction was applied to the model calculated structure factors using X-PLOR. In the final stages, only positional refinement using conjugate gradient minimization and individual *B*-factor refinement were done. PROCHECK (Laskowski et al., 1993) was used to determine areas of poor geometry. For the purpose of locating bound solvent molecules, MAPMAN was used to select peaks of height 3.5 standard deviations above the mean from a difference map, and X-PLOR was used to eliminate those peaks that were not within 3.5 Å of a protein nitrogen or oxygen atom. O was used to manually view and accept water sites. The final model consisted of residues 3 through 319 and 23 bound water molecules ($R_{work} = 0.26$, $R_{free} = 0.35$; 20–2.8 Å).

A difference map of the form $(F_{NAD} - F_c)\alpha_{calc}$, using the native protein model to calculate structure factors and phases, was calculated using X-PLOR. The map showed good density for the adenosine moiety and connected phosphate group of NAD but poor density for the remainder of the molecule. A model of NAD was fit to density. For the protein–NAD complex, positional refinement was done using conjugate gradient minimization with X-PLOR. An anisotropic *B*-factor correction was made to the observed modulus structure factors, and a bulk solvent correction was applied to the calculated structure factors using X-PLOR. Group *B*-factors were also refined. The groups chosen were the main-chain atoms of each amino acid residue, the side-chain atoms of each residue, the atoms of the adenosine and phosphate moiety of NAD, and the atoms of nicotinamide and phosphate moiety. The final model had an R_{work} of 0.25 and an R_{free} of 0.36 (20–3.0 Å).

Least-squares superpositions of molecules were made with O. Molecular drawings were made with MOLSCRIPT (Kraulis, 1991).

Accession number

The coordinates have been deposited with the Protein Data Bank. The PDB ID codes are: 1EDZ and 1EE9.

Acknowledgments

This work was supported by grant GM 30048 from the National Institutes of Health and by grants from the Foundation for Research, the Welch Foundation, and grant ARP-119 from the Texas Higher Education Board.

We thank Russell Ward and Elisabeth Schelp for technical assistance in the preparation of yMTD. We thank Dr. R.M. Sweet and Salvatore Sclafani for technical assistance at beamline X12-C in the National Synchrotron Light Source, Brookhaven National Laboratory.

Diffraction data for this study were collected at Brookhaven National Laboratory in the Biology Department single-crystal diffraction facility at beamline X12-C in the National Synchrotron Light Source. This facility is supported by the United States Department of Energy Offices of Health and Environmental Research and of Basic Energy Sciences under prime contract DE-AC02-98CH10886, by the National Science Foundation, and by National Institutes of Health Grant 1P41 RR12408-01A1.

References

Allaire M, Li Y, Mackenzie RE, Cygler M. 1998. The 3-D structure of a folate-dependent dehydrogenase/cyclohydrolase bifunctional enzyme at 1.5 Å resolution. *Structure 6*:173–182.

Appling DR, West MG. 1997. Monofunctional NAD-dependent, 5,10-methylenetetrahydrofolate dehydrogenase from *Saccharomyces cerevisiae*. *Methods Enzymol 281*:178–188.

Barlowe CK, Appling DR. 1990. Isolation and characterization of a novel eukaryotic monofunctional NAD^+-dependent 5,10-methylenetetrahydrofolate dehydrogenase. *Biochemistry 29*:7089–7094.

Birktoft JJ, Rhodes G, Banaszak LJ. 1989. Refined crystal structure of cytoplasmic malate dehydrogenase at 2.5-Å resolution. *Biochemistry 2*:6065–6081.

Brünger AT. 1992. *X-PLOR version 3.1: A system for X-ray crystallography and NMR*. New Haven, Connecticut: Yale University Press.

Brünger AT. 1993. Assessment of phase accuracy by cross validation: The free *R* value. *Acta Crystallogr D4*:129–147.

CCP4 (Collaborative Computational Project Number 4). 1994. The CCP4 suite: Programs for protein crystallography. *Acta Crystallogr D5*:760–763.

Hoffman DW, Davies C, Gerchman SE, Kycia JH, Porter SJ, White SW, Ramakrishnan V. 1994. Crystal structure of prokaryotic ribosomal protein L9: A bi-lobed RNA-binding protein. *EMBO J 13*:205–212.

Jones TA, Zou JY, Cowan SW, Kjeldgaard M. 1991. Improved methods for building models in electron density maps and the location of errors in these models. *Acta Crystallogr A4*:110–119.

Kleywegt GJ, Jones TA. 1996. xdlMAPMAN and xdlDATAMAN—Programs for reformatting, analysis, and manipulation of biomolecular electron-density maps and reflection data sets. *Acta Crystallogr D5*:826–828.

Kraulis PJ. 1991. MOLSCRIPT: A program to produce both detailed and schematic plots of protein structure. *J Appl Crystallogr 2*:946–950.

Laskowski RA, MacArthur MW, Moss DS, Thornton JM. 1993. PROCHECK: A program to check the stereochemical quality of protein structures. *J Appl Crystallgr 2*:283–291.

Lunin VY, Skovoroda TD. 1995. *R*-free likelihood-based estimates of errors for phases calculated from atomic models. *Acta Crystallogr A5*:880–886.

MacKenzie RE. 1984. Biogenesis and interconversion of substituted tetrahydrofolates In: Blakely R, Benkovic S, eds. *Folates and pterins: Chemistry and biochemistry of folates*. New York: Wiley and Sons. pp 255–306.

MacKenzie RE. 1997. Mitochondrial NAD-dependent methylenetetrahydrofolate dehydrogenase-methenyltetrahydrofolate cyclohydrolase. *Methods Enzymol 281*:171–177.

Mejia NR, MacKenzie RE. 1985. NAD-dependent methylenetetrahydrofolate dehydrogenase is expressed by immortal cells. *J Biol Chem 260*:14616–14620.

Monzingo AF, West MG, Schelp E, Appling DR, Robertus JD. 1996. Crystallization of the NAD-dependent 5,10-methylenetetrahydrofolate dehydrogenase from *Saccharomyces cerevisiae*. *Proteins Struct Funct Genet 2*:481–482.

Nicholls A, Sharp KA, Honig B. 1991. Protein folding and association: Insights from the interfacial and thermodynamic properties of hydrocarbons. *Proteins Struct Funct Genet 11*:281–293.

Otwinowski Z, Minor W. 1997. Processing of X-ray diffraction data collected in oscillation mode. *Methods Enzymol 27*:307–326.

Pawelek PD, MacKenzie RE. 1998. Methenyltetrahydrofolate cyclohydrolase is rate limiting for the enzymatic conversion of 10-formyltetrahydrofolate to 5,10-methylenetetrahydrofolate in bifunctional dehydrogenase-cyclohydrolase enzymes. *Biochemistry 3*:1109–1115.

Ramakrishnan V, Biou V. 1997. Treatment of MAD data as a special case of MIR. *Methods Enzymol 27*:538–555.

Robinson DR. 1971. The nonenzymatic hydrolysis of N^5,N^{10}-methenyltetrahydrofolic acid and related reactions. *Methods Enzymol 1*:716–725.

Rossmann MG, Lilias A, Branden CI, Banaszak LK. 1975. Evolutionary and structure relationships among dehydrogenases. In: Boyer PD, ed. *The enzymes: Oxidation-reduction*. New York: Academic Press. pp 61–102.

Schirch L. 1984. Folates in serine and glycine metabolism. In: Blakley RL, Benkovic SJ, eds. *Folates and pterins*. New York: Wiley. pp 399–431.

Shen BW, Dyer DH, Huang JY, D'Ari L, Rabinowitz J, Stoddard BL. 1999. The crystal structure of a bacterial, bifunctional 5,10 methylene-tetrahydrofolate dehydrogenase/cyclohydrolase. *Protein Sci 8*:1342–1349.

Terwilliger TC, Berendzen J. 1999. Automated structure solution for MIR and MAD. *Acta Crystallogr D5*:849–861.

Urzhumtsev AG, Skovoroda TD, Lunin VY. 1996. A procedure compatible with X-PLOR for the calculation of electron-density maps weighted using an *R*-free-likelihood approach. *J Appl Crystallogr 2*:741–744.

West MG, Barlowe CK, Appling DR. 1993. Cloning and characterization of the *Saccharomyces cerevisiae* gene encoding NAD-dependent 5,10-methylenetetrahydrofolate dehydrogenase. *J Biol Chem 268*:153–160.

West MG, Horne DW, Appling DR. 1996. Metabolic role of cytoplasmic isozymes of 5,10-methylenetetrahydrofolate dehydrogenase in *Saccharomyces cerevisiae*. *Biochemistry 3*:3122–3132.

Yang X-M, MacKenzie RE. 1993. NAD-dependent methylenetetrahydrofolate dehydrogenase-methenyltetrahydrofolate cyclohydrolase is the mammalian homolog of the mitochondrial enzyme encoded by the yeast MIS1 gene. *Biochemistry 32*:11118–11123.